Synergies between H-NBI fast-ions and ICRF heating in the non-activated operational phase of ITER

R. Bilato[1], A.R. Polevoi[2], M. Schneider[2], M. Brambilla[1], E. Fable[1], M. Weiland[1], Ye.O. Kazakov[3], E. Lerche[3], A. Loarte[2], J. Ongena[3], S.D. Pinches[2], D. Van Eester[3]

[1] *Max-Planck Institut für Plasmaphysik - Germany, EURATOM Ass.*

[2] *ITER Organization, Route de Vinon sur Verdon, CS 90 046, 13067 St Paul-lez-Durance Cedex, France*

[3] *LPP-ERM/KMS, Association Eurofusion-Belgian State, TEC partner, Brussels, Belgium*

1. Introduction - To access type-I ELMy H-mode scenarios in ITER during the Pre-fusion Power Operation 2 (PFPO-2) with hydrogen (H) and helium (He^4) plasmas, it is necessary to operate at reduced confining magnetic field to exceed the power threshold for the L-H transition [1]. During this operation phase it is planned the commissioning of the baseline auxiliary power heating, made up of 33 MW of Neutral Beam Injection (NBI) (hydrogen at a maximum injection energy of 870 keV), 20 MW of ECRF and 20 MW of ICRF (f=40-55 MHz) [2]. Depending on the ICRF frequency and the confining magnetic field, hydrogen can resonate at its harmonic cyclotron frequency (1^{st} at half-field (2.65 T), $\omega = \Omega_{cH}$, and 2^{nd} at one-third field (1.8 T), $\omega = 2\Omega_{cH}$, with Ω_{cH} the angular hydrogen cyclotron frequency) with the launched ICRF waves [2]. In particular, the NBI-ICRF synergies when the NBI species resonates at its 1^{st} harmonic using three-ion scenarios have been recently observed in JET [3].

In the next section, the simulations tools used in this analysis are briefly described, and the results of parametric scans in frequency and H concentration are presented in Section 3. Conclusions are drawn in Section 4.

2. Simulation Tools and Target Plasma Parameters - To investigate NBI-ICRF synergies, the toroidal axisymmetric full-wave `TORIC` code is used to simulate propagation and absorption of Radio Frequency (RF) waves in the Ion Cyclotron Range of Frequencies (ICRF), and the `SSFPQL` code is used for the steady-state solution of the surface-averaged kinetic equation of all ion heated species [5]. `SSFPQL` solves the kinetic equation in the limit of zero-orbit-width approximation, but accounts for trapping effects in the description of wave-particle resonance, and can deal with the simultaneous presence of NBI sources and ICRF heating [4]. The coefficients of the wave equation solved by `TORIC` are calculated from the numerical solutions of `SSFPQL` [5]. The nonlinear iteration between `TORIC` and `SSFPQL` is controlled by a modified Anderson algorithm, and convergence is achieved when `TORIC` and `SSFPQL` predict absorption profiles which differ less than a chosen threshold (here set to 0.5%) [5].

The target plasma parameters are calculated with `ASTRA` transport code [6]: The transport coefficients are set to provide a pedestal height $p_{e,ped} = p_{ped}/2$ according to `EPED1&SOLPS` scaling [7], with boundary conditions from `SOLPS` scaling [8]; the transport model for heat and particle is fitted to provide $\tau_E = 0.75\tau_{98,y2,D}$, $\chi_i = 2\chi_e$ in the core and $\chi_i = \chi_e$ at ETB, and $D = 0.1(\chi_i + \chi_e)$, $v = Dx/a$ [9]. In the `ASTRA` simulation the auxiliary heating system consists of

20 MW of ECRH, 16.5 MW on-axis and 16.5 MW off-axis of H-NBI with $E_{\mathrm{NBI}} = 870$ MeV, and 20 MW of on-axis ICRF. This target plasma is kept unchanged in TORIC-SSFPQL simulations discussed in the following.

3. Frequency and H-Concentration Scans - In the frequency window foreseen in ITER, the 1st-harmonic resonance of hydrogen at half-field (2.65 T) is at $r/a \approx 0.03$ on the low-field side for $f = 40$ MHz and at $r/a \approx 0.8$ on the high-field side for $f = 53$ MHz. ICRF scenarios for ITER half-field phase in H and He^4 plasmas have been investigated at JET [10]. The simultaneous presence of NBI has an impact on the profiles of directly absorbed ICRF power, shown in fig. 1 at 40 MHz, with 5% of H and for $[0, \pi/2, \pi, 3\pi/2]$ (current-drive), left, and $[0, \pi, 0, \pi]$ (heating), right, antenna phasing. These profiles are obtained by summing over the entire spectrum in n_φ (fig. 2), as calculated by TORIC at convergence. The Doppler shift associated to the injection energy of the H-NBI species resonating with ICRF waves [11] deforms substantially the H-absorption profile. This deformation is larger in correspondence of the maximum of NBI deposition (magenta line). Direct RF-power deposition profiles are broader for heating than for current-drive phasings because of the larger contributions from higher n_φ in the antenna spectrum. In fact, Doppler shift depends on the parallel component of the wave vector, which in turn increases with n_φ. In studying the impact of RF frequency and H concentration on the RF power

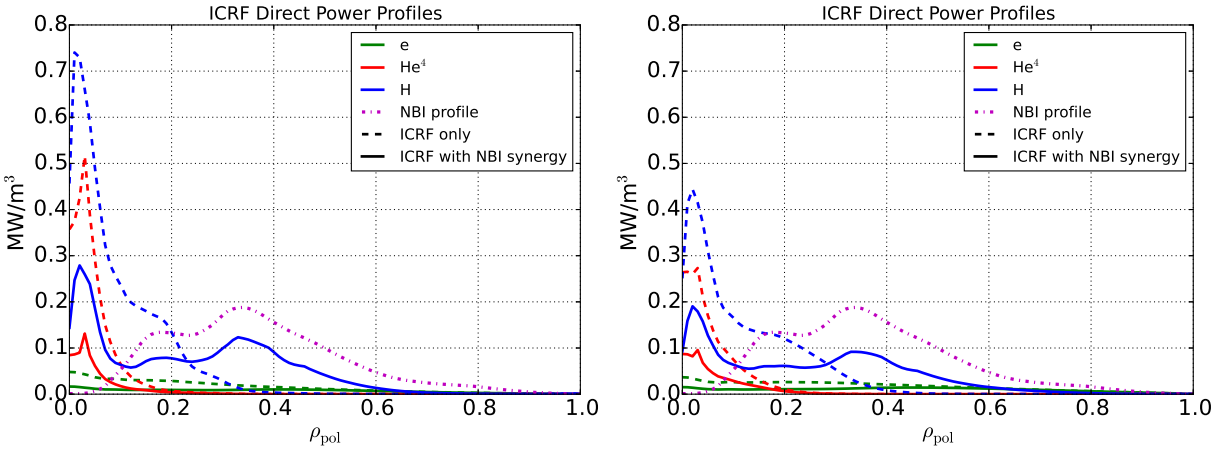

Figure 1: *Absorbed power profiles at convergence:* $[0, \pi/2, \pi, 3\pi/2]$ *(left) and* $[0, \pi, 0, \pi]$ *(right) phasing.*

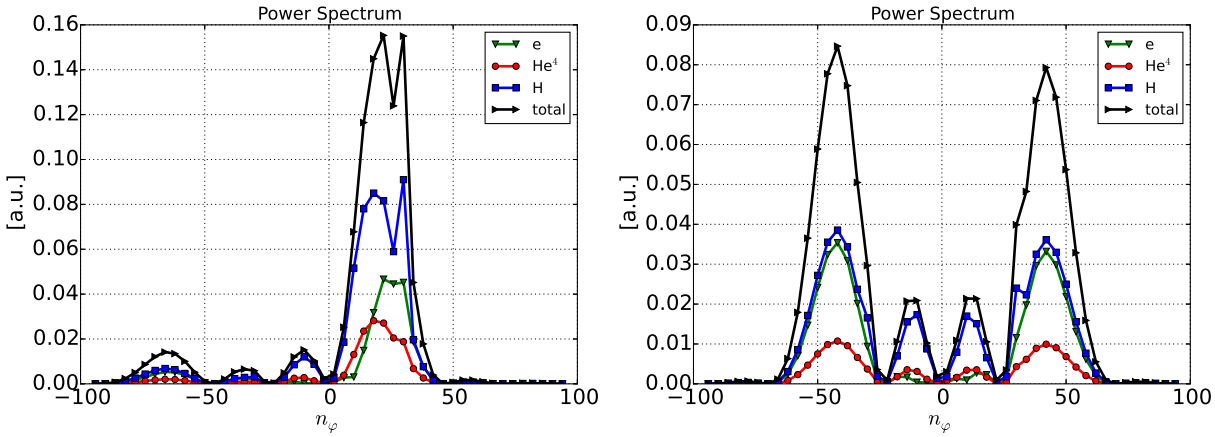

Figure 2: *Power spectra calculated by* TORIC*:* $[0, \pi/2, \pi, 3\pi/2]$ *(left) and* $[0, \pi, 0, \pi]$ *(right) phasing.*

repartition, only one n_φ is considered in TORIC simulations, and precisely $n_\varphi = 27, 50$, representative of the main peaks of current-drive and heating phasings, respectively. Figure 3(left) summarizes the results of the frequency scan assuming that only ICRF is on and with 5% of H, typical value for ICRF minority heating scheme, and $n_\varphi = 27$. The dashed lines are the fraction of ICRF power directly absorbed by H (blue), He^4 (red) and electrons (green), with the coefficients of the wave equation solved by TORIC calculated with the distribution functions of SSFPQL at achieved convergence. The dotted lines are the results of the first run of TORIC as-

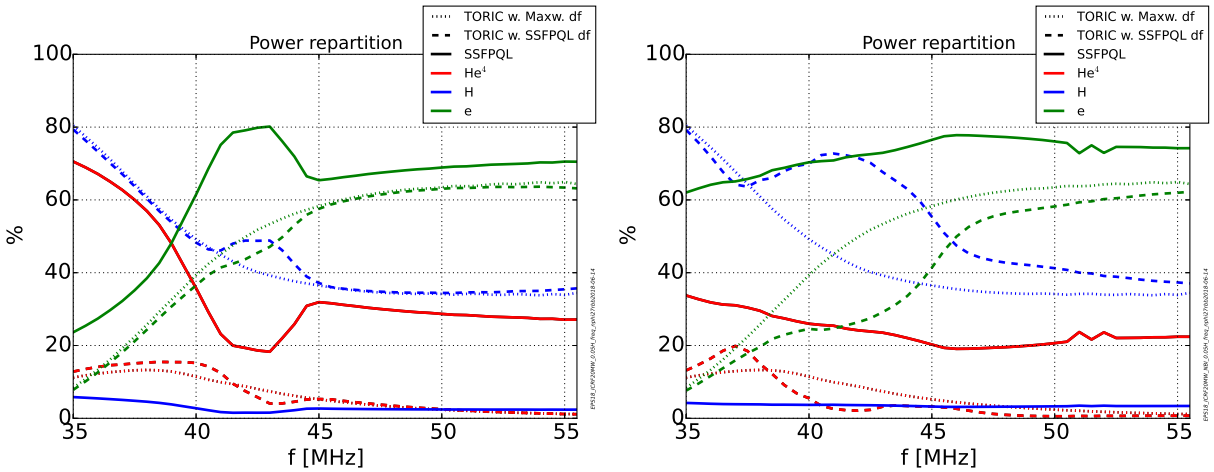

Figure 3: *Dotted and dashed lines refer to fractions of direct RF absorbed power with Maxwellians and* SSFPQL *distribution functions at convergence, respectively. Solid lines show the power fractions after collisional redistribution* SSFPQL. *The left plot is for ICRF only, whereas the right one for ICRF+NBI.*

suming Maxwellian distributions, and the differences with the converged profiles (dashed lines) are due to the Doppler broadening of the H absorption line caused by the suprathermal tail produced by ICRF itself. These differences are largest when the H-1st-harmonic IC resonance falls in the plasma core. The solid lines show the fraction of ICRF power that eventually goes to the background species via collisions, as calculated by SSFPQL. In the simultaneous presence of NBI, the power repartition is shown in fig. 3(right). The impact of NBI on direct RF absorption is clear from the comparison of dashed lines of both plots: H absorption is modified when the IC resonance falls in the region of large NBI deposition. The increase of H absorption has an indirect impact also on the other species (red and green lines) because of the competition with RF-wave damping by electrons and He^4. The solid lines in fig. 3(right) show the sum of ICRF and NBI contributions for each plasma species. For reference, in the case of NBI only, SSFPQL predicts that 80% of the NBI power goes to electrons, 18% to He^4 and only 2% to H. Figure 4 shows the same curves of fig. 3 when the H concentration is varied at 40 MHz. When H concentration is low (<10%), there is dominant heating of the minority species, H (dotted/dashed-blue line); as the concentration is increased the scenario moves to the mode conversion regime, where ion Bernstein waves (IBW) are excited at the ion-ion resonance, and IBWs are preferentially absorbed by electrons (dotted/dashed-green line). Also in this case, the impact of H-NBI on increasing RF-power directly absorbed by H is clear from the comparison of the blue-dashed lines in the right and left plots of fig. 1. This effect decreases when H becomes the main ion

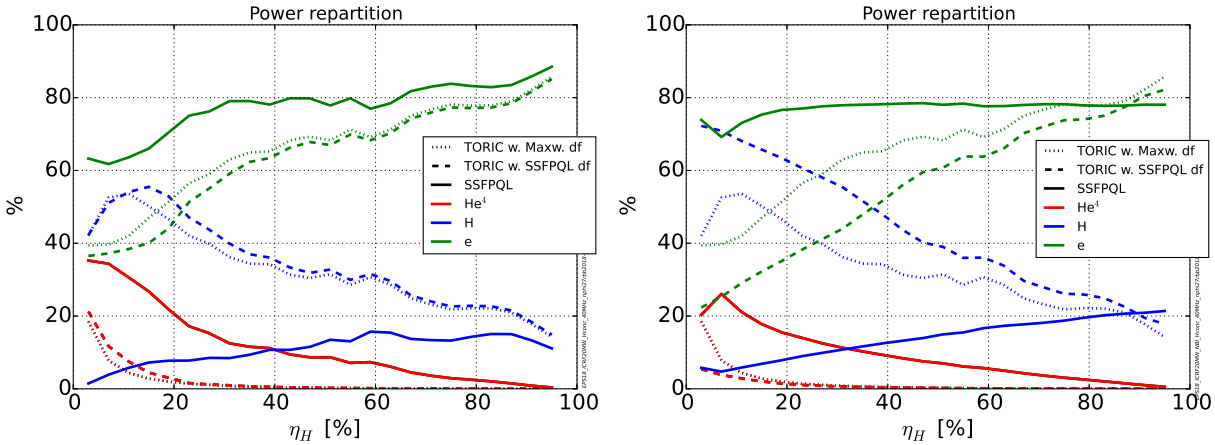

Figure 4: *Same of figure 3 as function of H concentration.* $\eta_H = n_H/n_e$.

species because of the E_+ screening by H at $\omega = \Omega_{\mathrm{cH}}$ [10]. Since ITER lacks an efficient ICRH absorption scenario at half-field in H-majoriy plasmas, an optional scheme with off-axis He^3 minority heating in H(He^4) ($\approx 10\%$ of He^4) plasmas, promising for H-mode access studies in H majority plasmas at $B_0 = 3.0 \div 3.3$ T, has been recently proposed in [12].

4. Conclusions - H–NBI heating increases the fraction of ICRF power directly absorbed by hydrogen, and substantially broadens the profile of ICRF power absorbed by hydrogen. This becomes less pronounced when the H concentration is increased. Although the negative impact of NBI heating on high-Z impurity (e.g. tungsten) accumulation in the plasma core is expected to be strongly reduced by the low NBI particle source in ITER core [13], the synergy between ICRF and NBI favorably increases the ratio of the electron, P_e, to total, $P_T = P_e + P_i$, integrated auxiliary heating, $P(x) = \int_0^x (\mathrm{d}P_{IC}/\mathrm{dV})\,\mathrm{d}V$. This ratio is shown in fig. 5 for the cases with (solid) and without (dashed) ICRF-NBI synergies, for $[0, \pi/2, \pi, 3\pi/2]$ and $[0, \pi, 0, \pi]$ antenna phasings at 40 MHz and 5% of H.

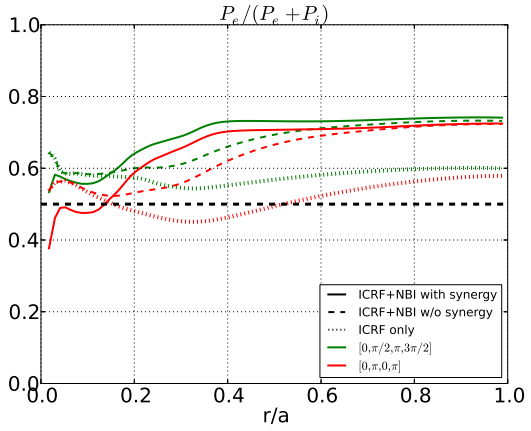

Figure 5: *Ratio of electron to total integrated power (freq. 40 MHz and 5% of H).*

ITER is the Nuclear Facility INB no. 174. The views and opinions expressed herein do not necessarily reflect those of the ITER Organization.

References

[1] Y. Martin, *et al.*, J. of Physics: Conf. Series 123 (2008) 012033.
[2] M. Schneider, *et al.*, Proc. 44th EPS Conf. on Plasma Physics, (2017) P5.153.
[3] J. Ongena, *et al.*, EPJ Web Conf., 157 (2017) 02006.
[4] R. Bilato, *et al.*, Nucl. Fusion, 51 (2011) 103034.
[5] M. Brambilla, R. Bilato, Nucl. Fusion, 49 (2009) 85004.
[6] G. Pereverzev, P. N. Yushmanov, IPP Report 5/98 (2002).
E. Fable, *et al.*, Plasma Phys. Control. Fusion, 55 (2013) 124028.
[7] A.R. Polevoi, *et al*, Nucl. Fusion, 57 (2017) 022014.
[8] A.S. Kukushkin, Nucl. Fusion, 53 (2013) 123025.
[9] A.R. Polevoi, *et al.*, Proc. 39th EPS Conf. on Plasma Physics, (2012) P4.032.
[10] E. Lerche, *et al*, AIP Conference Proceedings, 1406 (2011) 245.
[11] E. Lerche, *et al*, Plasma Phys. Control. Fusion, 51 (2009) 044006.
[12] M. Schneider, *et al.*, EPJ Web Conf., 157, (2017) 03046.
[13] C. Angioni, *et al.*,Nucl. Fusion, 57 (2017) 056015.